Liquid Crystals
Publication details, including instructions for authors and subscription information:
http://www.informaworld.com/smpp/title~content=t713926090

Electron beam irradiation-induced transformations in the electrical properties of 4'-octyl-4-cyanobiphenyl (8CB)

Rohit Verma[ab]; R. Dhar[ab]; V. K. Agrawal[b]; M. C. Rath[c]; S. K. Sarkar[c]; V. K. Wadhawan[d]; R. Dabrowski[e]
[a] Materials Research Laboratory, Physics Department, Ewing Christian College, University of Allahabad, Allahabad, India [b] Physics Department, University of Allahabad, Allahabad-211002, India [c] Radiation and Photochemistry Division, Bhabha Atomic Research Centre, Trombay, Mumbai-400085, India [d] Solid State Physics Division, Bhabha Atomic Research Centre, Trombay, Mumbai-400085, India [e] Institute of Chemistry, Military University of Technology, 00-908-Warsaw, Poland

To cite this Article Verma, Rohit , Dhar, R. , Agrawal, V. K. , Rath, M. C. , Sarkar, S. K. , Wadhawan, V. K. and Dabrowski, R.(2009) 'Electron beam irradiation-induced transformations in the electrical properties of 4'-octyl-4-cyanobiphenyl (8CB)', Liquid Crystals, 36: 9, 1003 — 1014
To link to this Article: DOI: 10.1080/02678290903220972
URL: http://dx.doi.org/10.1080/02678290903220972

Liquid Crystals,
Vol. 36, No. 9, September 2009, 1003–1014

Taylor & Francis
Taylor & Francis Group

Electron beam irradiation-induced transformations in the electrical properties of 4'-octyl-4-cyanobiphenyl (8CB)

Rohit Verma[a,b], R. Dhar[a,b]*, V.K. Agrawal[b], M.C. Rath[c], S.K. Sarkar[c], V.K. Wadhawan[d] and R. Dabrowski[e]

[a]*Materials Research Laboratory, Physics Department, Ewing Christian College, University of Allahabad, Allahabad-211003, India;* [b]*Physics Department, University of Allahabad, Allahabad-211002, India;* [c]*Radiation and Photochemistry Division, Bhabha Atomic Research Centre, Trombay, Mumbai-400085, India;* [d]*Solid State Physics Division, Bhabha Atomic Research Centre, Trombay, Mumbai-400085, India;* [e]*Institute of Chemistry, Military University of Technology, 00-908-Warsaw, Poland*

(Received 5 January 2009; final form 30 July 2009)

Changes in the dielectric and thermodynamical properties of electron beam-irradiated 4′-octyl-4-cyanobiphenyl (8CB) were studied. Irradiation-induced changes in the phase transition temperature, dielectric anisotropy, relaxation frequency and activation energy of an observed non-collective relaxation mode corresponding to molecular rotation about the short axis were determined in both nematic and smectic A_d phases. In the nematic phase, dielectric anisotropy increased for a small dose but decreased for a relatively high dose, whereas the relaxation frequency increased due to the irradiation. The pure and irradiated samples were characterised by UV–visible spectroscopy, Fourier transform infrared spectroscopy, gas chromatography, gas chromatography coupled with mass spectroscopy and pulse radiolysis. The observed changes in the dielectric parameters are related to the detachment of the CN group from some of the 8CB molecules due to the electron beam irradiation.

Keywords: electron beam irradiation; dielectric parameters; relaxation frequency; UV-visible; Fourier transform infrared spectroscopy

1. Introduction

The understanding and application of liquid crystals are among the great scientific and technological achievements of the twentieth century, with integrated electronics and liquid crystal displays (LCDs) combining to enable the portable computing revolution. In 1911, Mauguin discovered and described the twisted nematic (TN) structure (*1*). Since the discovery of this mode, many materials have been tried for making twisted nematic displays but none was commercialised due to their instability and the small temperature range of the desired phase. A major breakthrough came when George W. Gray introduced cyanobiphenyl liquid crystals to the scientific community in 1973. These materials were stable over a large temperature range and proved to be excellent both for displays and for basic research. These and other developments made the TN-LCD the centre of the multimillion dollar international flat panel industry that we enjoy today.

Devices made up of the liquid crystalline materials (including LCDs) are often used, occasionally for a long time in different radiation-prone areas, such as nuclear installation centres and in various space applications. When these devices are used for a long time in such environments different types and doses of irradiation strongly affect these materials and create a malfunctioning of these devices. Some of the earlier studies on the effect of irradiation of various types and doses on the properties of liquid crystalline material (*2–10*) suggest that generally different phase transition temperatures are lowered which causes the stability of the phases to be reduced, AC and DC conductivities are increased (*2–7*), which degrade the dielectric properties of the material, and transition enthalpies and entropies are increased (*6*, *7*). In an earlier publication, we found that besides the above changes, threshold voltages are increased while the switching voltages are decreased (*8*). Therefore, it is important to study how and to what extent different types and doses of irradiation affect the different properties of these materials.

As discussed above, cyanobiphenyls, especially 4′-pentyl-4-cyanobiphenyl (5CB), were one of the first base materials to be commercialised for display purposes in TN-LCDs due to their low transition temperature range, good chemical stability and high dielectric anisotropy. In our recent publications, we have reported the effect of electron irradiation on the electro-optical and dielectric properties of 5CB (*8*, *9*). In the present work, we report the effect of electron beam irradiation on another homologous member, i.e. 4'-octyl-4-cyanobiphenyl (8CB). At present, most of the physical properties of 8CB have been studied (*11–19*). It possesses a nematic phase in the temperature range 40.8–33.6°C and smectic A_d phase in the range 33.6–22.0°C. The material used for the present study was of 99% purity.

*Corresponding author. Email: dr_ravindra_dhar@hotmail.com

ISSN 0267-8292 print/ISSN 1366-5855 online

DOI: 10.1080/02678290903220972
http://www.informaworld.com

2. Experimental techniques

The liquid crystal sample 8CB was obtained from R. Dabrowski, Institute of Chemistry, Military University of Technology, Poland. Pure 8CB samples were irradiated by electron beam irradiation up to 15 kGy dose using a 7 MeV linear electron accelerator (LINAC) setup at the Bhabha Atomic Research Centre, Mumbai, India. The samples were put inside a 1-mm thick quartz cell for the electron beam irradiation study. Pulses of 2 μs duration were used. The temperature of the sample inside the cell was maintained just above the phase transition temperature in order to have a transparent medium. The samples were given various amounts of cumulative doses up to 15 kGy to measure steady-state optical absorption spectra using a conventional absorption spectrophotometer. This was performed to characterise the stable radiolytic products, if any, obtained by the electron beam irradiation. The absorbed dose was determined using a chemical dosimeter, 0.5 mM potassium thiocyanate aqueous solution in the cell, which was used for the liquid crystal samples. Further details of the spectroscopic studies are discussed elsewhere (*20*).

The thermodynamical study of the pure and irradiated samples was carried out on a differential scanning calorimeter (DSC) of NETZSCH (model DSC 200 F3, Maia). The DSC was allowed to run initially for first five cycles with the scan rate of 5°C min^{-1} in the range −15–60°C in order to stabilise the transition temperatures and transition enthalpies. Peak transition temperatures (Tp) were determined to an accuracy of 0.1°C, whereas transition enthalpies (ΔH) were determined to an accuracy better than 2% for fully grown peaks. However, for very weak peaks, uncertainties were large. Different mesophases of the pure and irradiated samples were identified from the texture study with the help of a CENSICO optical polarising microscope (OPM) (Central Scientific Instrument Corporation, Agra, India). The textures were acquired on computer by a CCTV camera (model MINTRON).

For the dielectric measurements electrical cells in the form of a parallel plate capacitor were prepared using indium tin oxide and gold-coated glass plates with a sheet resistance less than 25 Ω, as electrodes, using 10 and 40-μm wide spacers. The active capacitance (C_L) was determined by introducing an organic liquid of known dielectric constant, in this case cyclohexane, into the cell. Capacitance (C) and conductance (G) of the cell filled with material were determined in the frequency range 1 Hz to 35 MHz using an impedance/gain phase analyser (Hewlett Packard model HP4194A), Solartron (model SI-1260) coupled with a Solartron dielectric interface (model 1296) and N4L's phase-sensitive multi-meter (model PSM 1735). A measuring electric field of 0.5 V_{rms} was applied across the sample. Temperature of the sample for dielectric and optical texture studies was controlled with the help of a hot stage system (Instec model HS-1) having an accuracy of ±0.1°C and a resolution limit ±0.003°C. Temperature near the sample was determined by measuring the thermo-electromotive force of a copper-constantan thermocouple with the help of a six and half digit multimeter with an accuracy of ±0.1°C.

For analysis of the measured data, the dielectric spectra were fitted on a generalised Cole–Cole equation:

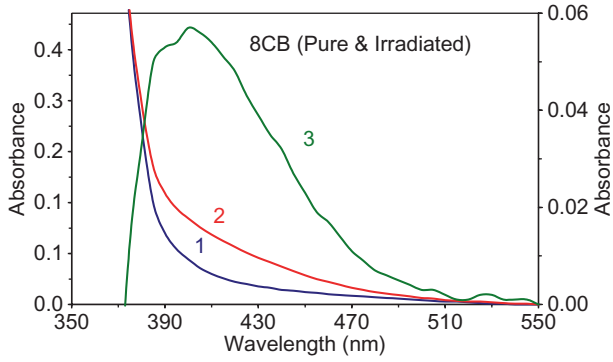

Figure 1. UV spectra: variation of absorbance (arbitrary unit) with wavelength (nm). Curves 1, 2 and 3 are the pure 8CB, 6 kGy irradiated 8CB and the difference between the absorbance of the irradiated and pure 8CB. Curves 1 and 2 are on the left vertical axis whereas curve 3 is on the right vertical axis.

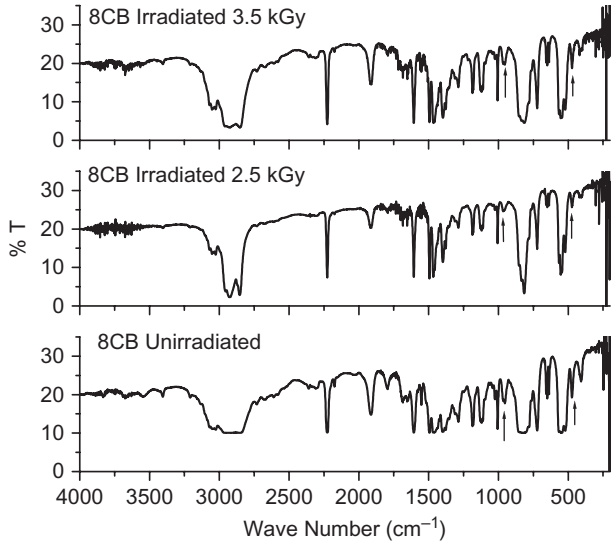

Figure 2. Fourier transform infrared spectra of the pure and electron beam-irradiated 8CB.

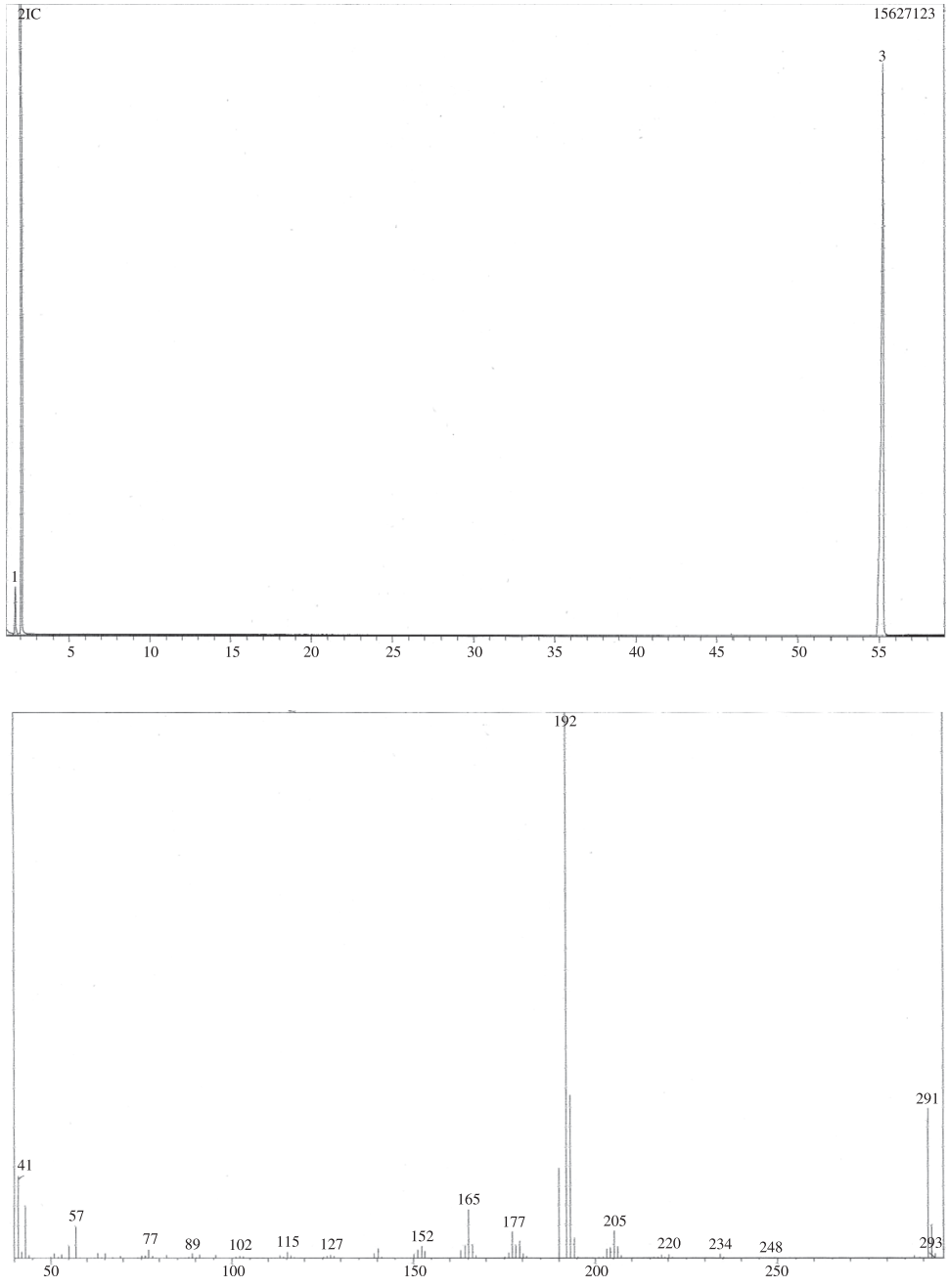

Figure 3. (a) Gas chromatogram (upper) and gas chromatogram coupled mass spectrum (lower) of Pure 8CB; (b) gas chromatogram (upper) and gas chromatogram coupled mass spectrum (lower) of the irradiated 8CB.

$$\varepsilon^* = \varepsilon' - j\varepsilon'' = \varepsilon'(\infty) + \sum \frac{(\Delta\varepsilon)}{1 + (j\omega\tau)^{(1-\alpha)}} + \frac{A}{\omega^n} - j\frac{\sigma_{ion}}{\varepsilon_0\,\omega^k} - jB\omega^m \quad (1)$$

where $\varepsilon'(\infty)$ is the high-frequency limiting value of the relative dielectric permittivity, $\Delta\varepsilon$, τ and α are dielectric strength, relaxation time and distribution parameter ($0 < \alpha < 1$), respectively. The third term of Equation (1) represents the contribution of the electrode polarisation of capacitance at low frequency (*21*), where A and n are fitting parameters. $\sigma_{ion}/\varepsilon_0\omega^k$ accounts for the contribution due to ionic conductivity (σ_{ion}), k is a fitting parameter and usually is 1 for dc conductivity. ε_0 (= 8.85 pF/m) is the free space permittivity. The measured dielectric absorption $\varepsilon''_{\|}$ may contain a contribution above 100 kHz due to finite

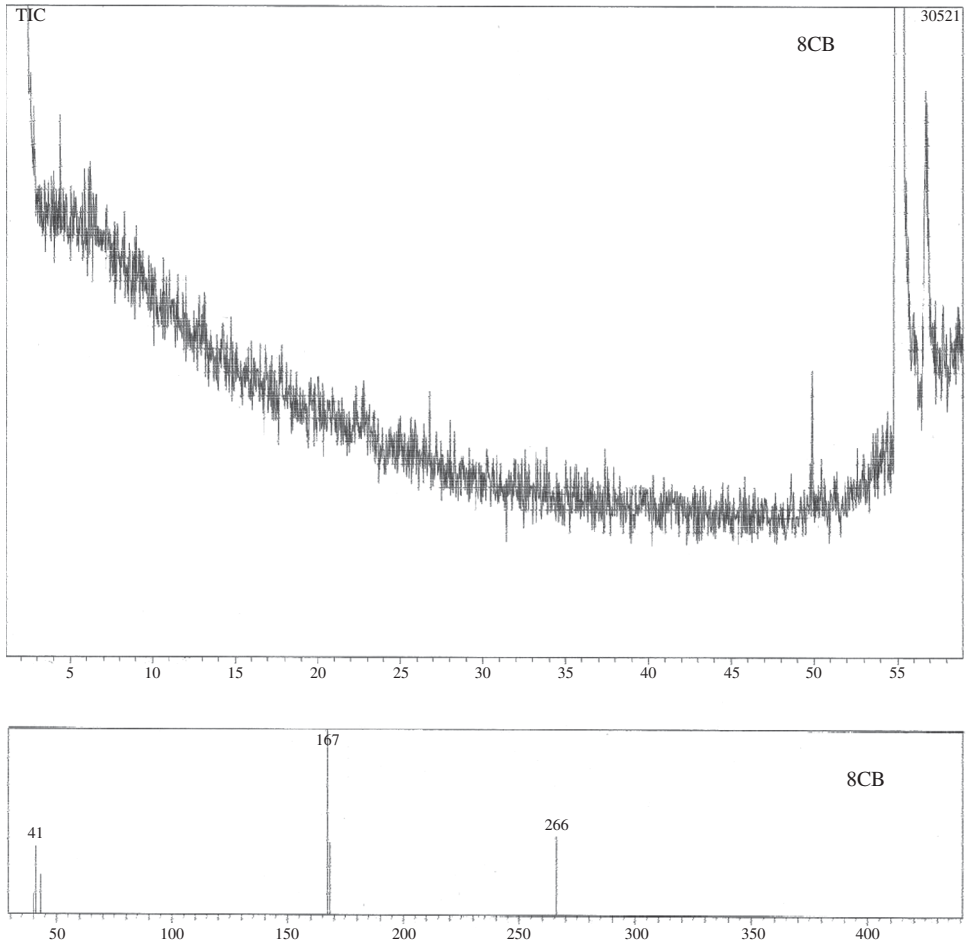

Figure 3. (*Continued*)

resistance of the electrodes and lead inductance (*22*). An additional imaginary term $B\omega^{m}$ is empirically added in Equation (1) to partially account for this effect (*23*, *24*), where B and m are fitting constants. Permittivity and loss values were determined with a maximum uncertainty of 2%. The uncertainty in the determination of the dielectric strength and relaxation frequency by the above-mentioned fitting process is well within ±5%. Further details about the experimental techniques used for the dielectric measurements are given in previous publications (*25–27*).

3. Results and discussion

The UV spectra acquired in the isotropic liquid phase of pure and irradiated 8CB (acquired within 30 minutes of irradiation) is shown in Figure 1. It can be seen that there is an additional absorption peak at 400 nm (corresponding energy 3.1 eV) in the irradiated 8CB spectrum, which becomes visible on subtracting the absorbance of the pure sample from the 6 kGy irradiated sample. However, we noticed a long-term ageing affect with this peak and it dwindles with time. Fourier transform infrared spectra showing the variation of transmittance with wave number (cm^{-1}) of pure and irradiated 8CB are shown in Figure 2. IR spectra of the irradiated sample show that intensities of the peaks at 408, 475 (C–C bending) and 957 cm^{-1} (C–C stretching) are decreasing. These peaks belong to the C–C bond between the CN group and benzene ring of the core group of 8CB. This indicates that there could be a detachment of the CN group from some of the 8CB molecules. Intensity of another weak peak at 1790 cm^{-1} slightly decreases on irradiation. This peak belongs to the second order harmonic peak of CH benzene out of phase vibration.

Pure and irradiated samples were analysed by gas chromatography (GC) and gas chromatography coupled with mass spectroscopy (GCMS). The gas chromatograms and the mass spectra of the pure and irradiated 8CB samples are shown in Figure 3(a) and (b), respectively. The GC and GCMS experiments

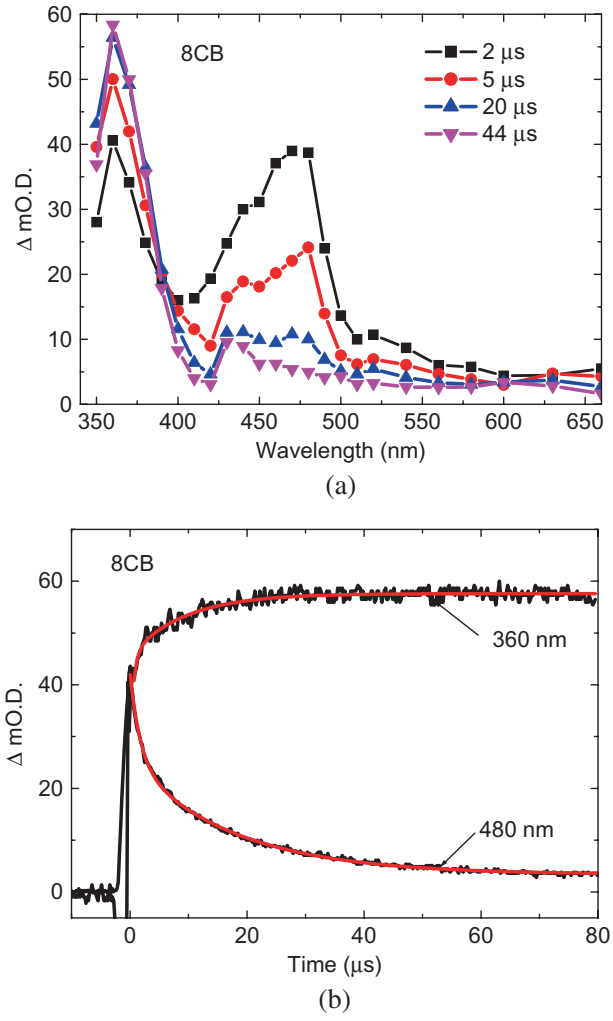

Figure 4. (a) Time-resolved transient absorption spectra of the electron beam-irradiated 8CB obtained from the pulse radiolysis experiments performed with the linear electron accelerator setup. The times at which the spectra were obtained are indicated in the figures. (b) Kinetic profiles obtained from the pulse radiolysis experiments performed with the linear electron accelerator setup at various probe wavelengths.

were carried out under identical conditions. The chromatograms are shown at different magnifications in order to demonstrate the additional GC peaks of the irradiated samples. The non-irradiated GCMS shows two major peaks at m = 291 and 192, which correspond to the molecular peak (291) and the fragmented peak (192), i.e. the C_7H_{15} group detached from 8CB. The irradiated GCMS also shows two major peaks at m = 266 and 167, both of which correspond to the detachment of a CN group (–26) with the addition of a proton (+1) from the matrix. Hence these results suggest that there could be CN group detachment due to irradiation of the 8CB compound.

The dynamics of the radiolysis of liquid samples is often studied by use of a pulse radiolysis setup, such as a LINAC. We heated the sample above its clearing temperature in order to keep it in the transparent isotropic liquid phase. In this condition, the sample was irradiated by 2-µs 7-MeV electron pulses. The transient absorption spectra were obtained by probing the radiolysed sample by a xenon flash lamp at a 90° angle to the irradiation beam. The transient absorption spectra thus obtained for the sample is shown in Figure 4(a). It is clear from the spectrum that there exists three absorption peaks at 360, 440 and 480 nm. The initial 440-nm and 480-nm peaks vanish with the growth of the 360-nm absorption peak for the 8CB sample.

The kinetics of the transient species at these wavelengths were investigated. The time-resolved transient absorption profiles obtained at the absorption peak positions were nicely fitted with a bi-exponential fitting equation. The kinetic parameters are listed in Table 1. The kinetic profiles along with the fitted curves are shown in Figure 4(b). The transient species having an absorption maximum at 480 nm, decays with two time constants, 5.75×10^5 s^{-1} (48%) and 5.65×10^4 s^{-1} (52%). The transient species having an absorption maximum at 360 nm grows with two time constants, 1.65×10^6 s^{-1} (larger component) and 1.10×10^5 s^{-1} (smaller component). It is now clear from these transient data that the transient radiolytic products (TP) having absorption maxima at 420 nm and 480 nm are converted to another TP, which has already been formed during the radiolysis and has an absorption maximum at 360 nm. Thus there are three TPs formed due to electron beam radiolysis. Overall the radiolysis process of the material is represented in Scheme 1. The final radiolytic product demonstrates absorption at 400 nm as shown in Figure 1.

Various transition temperatures of the pure and the irradiated samples were determined by OPM and DSC studies. The DSC thermograms for the heating and cooling cycles of the pure and irradiated samples (at a scan rate of 5 K min^{-1}) are shown in Figure 5. The OPM and DSC studies suggest that the transition process slows with the increasing dose of irradiation. Therefore, transition width increases with increasing dose of irradiation. The studies also suggest that all the transition temperatures are lowered due to irradiation (see Figure 5) in the cooling cycle. From the OPM and dielectric studies, we found that for pure 8CB, isotropic to nematic transition temperature was 40.8°C and nematic to smectic A_d transition temperature was 33.6°C. For the 6 kGy irradiated sample, isotropic to nematic transition temperature was 40.2°C, whereas the nematic to smectic A_d transition temperature occurred at 33.2°C. In the case of the 15 kGy irradiated sample, isotropic to nematic transition

Table 1. Kinetic parameters obtained from the transient profiles after fitting with a double exponential fitting equation, $y = y_0 + a_1 \exp(-(x - x_0)/t_1) + a_2 \exp(-(x - x0)/t_2)$ for the irradiated sample of 8CB. Here $1/t_1 = k_1$ and $1/t_2 = k_2$.

λ (nm)	y_0	x_0	a_1	k_1 (s^{-1})	a_2	k_2 (s^{-1})
360	0.0576	–4.275	–0.019	1.10×10^5*	–20.39	1.65×10^6
480	0.0034	–0.262	0.022 (52%)	5.65×10^4	0.02 (48%)	5.75×10^5

Note: *Rate constant for the formation of the transient species. Other rate constants represent the decay of the transient species.

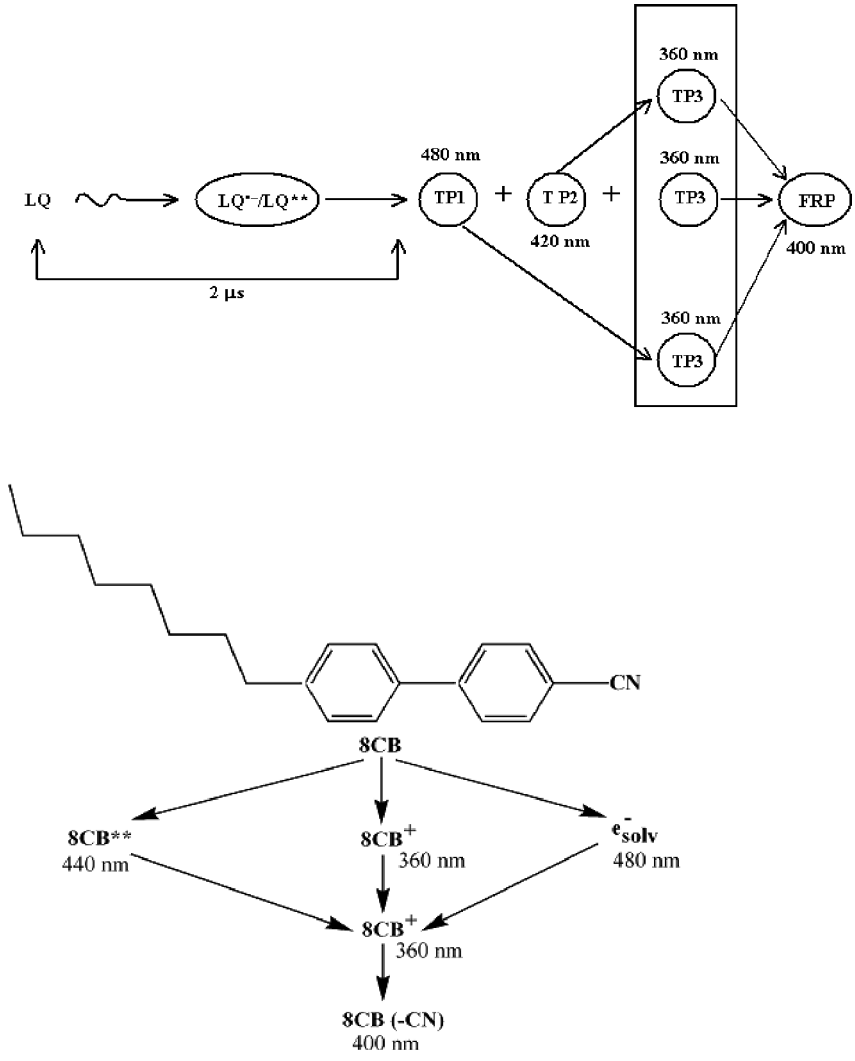

Scheme 1. A schematic representation of the radiolysis of the liquid crystal (LQ) sample, 8CB, leading to the formation of various transient products (TPs) and final radiolytic product (FRP). LQ^- and LQ^{**} represent the ionised and super-excited states of LQ. 8CB (-CN) represents the 8CB main chain without the CN group.

temperature was 37.8°C and nematic to smectic A_d transition temperature occurred at 30.8°C. OPM studies suggested that the isotropic-nematic transition starts at 38.1°C and completes at 33.8°C. Of course this interval is biphasic and thus width of the isotropic-nematic transition is large in the case of the 15 kGy irradiated sample.

The variation of the longitudinal ($\varepsilon'_{\parallel}$) and transverse ($\varepsilon'_{\perp}$) components of the relative dielectric permittivity of the pure, 6 kGy and 15 kGy irradiated samples are shown in Figure 6. Longitudinal ($\varepsilon'_{\parallel}$), transverse ($\varepsilon'_{\perp}$), average ($\varepsilon'_{ave} = (\varepsilon'_{\parallel} + 2\varepsilon'_{\perp})/3$) components of the relative dielectric permittivity, dielectric anisotropy ($\Delta\varepsilon'$) and ratio of dielectric anisotropy to

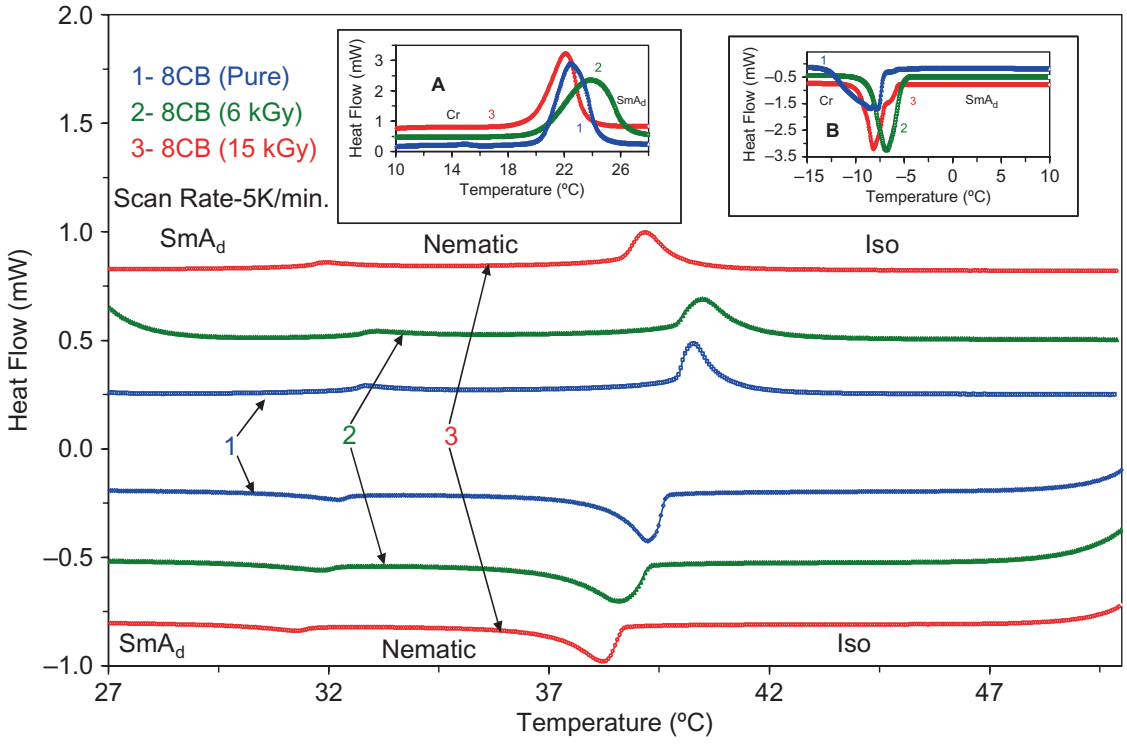

Figure 5. Differential scanning calorimetry thermograms for the heating and cooling cycles of pure and irradiated 8CB. Curves 1, 2 and 3 are for the pure, 6 kGy and 15 kGy irradiated 8CB, respectively. Insets A and B show the SmA$_d$-Cr transition of the pure and electron beam-irradiated 8CB in the heating and cooling cycles, respectively.

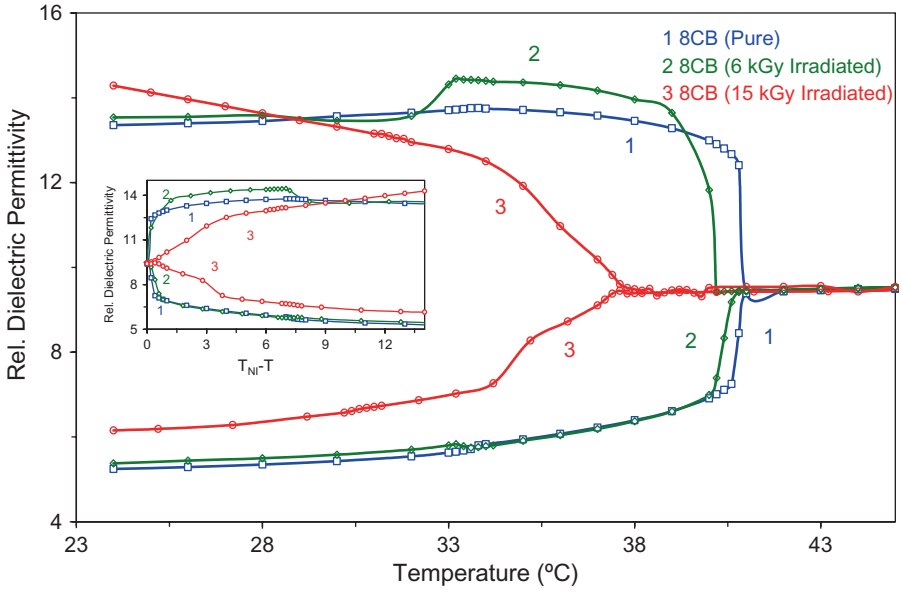

Figure 6. Temperature dependence of the longitudinal ($\varepsilon'_{\parallel}$) and transverse ($\varepsilon'_{\perp}$) components of the relative dielectric permittivity for the pure, 6 kGy and 15 kGy irradiated 8CB. The plots in the inset show the variation of the two components with common reduced temperature T_{NI}–T (°C). Curves 1, 2 and 3 are for the pure, 8CB, 6 kGy and 15 kGy electron beam-irradiated 8CB.

the transverse component of relative dielectric permittivity ($\Delta\varepsilon'/\varepsilon'_{\perp}$) in the smectic A$_d$ (at 24.0°C) and nematic (at 34.0°C) phases for the pure and irradiated samples are listed in Table 2. The values of $\varepsilon'_{\parallel}$ and $\varepsilon'_{\perp}$ for the pure 8CB material are in fair agreement with data in the literature (*11*, *12*). The dielectric results

Table 2. Variation of the longitudinal ($\varepsilon'_{\parallel}$), transverse ($\varepsilon'_{\perp}$) and average (ε' = ($\varepsilon'_{\parallel}$+ 2$\varepsilon'_{\perp}$)/3) components of the relative dielectric permittivity, dielectric anisotropy ($\Delta\varepsilon$') and ratio of dielectric anisotropy to the transverse component of the relative dielectric permittivity ($\Delta\varepsilon'/\varepsilon'_{\perp}$) in the smectic A_d (at 24.0°C) and nematic (at 34.0°C) phases

	Dose (kGy)	$\varepsilon'_{\parallel}$	$\varepsilon'_{\perp}$	ε' = ($\varepsilon'_{\parallel}$+ 2$\varepsilon'_{\perp}$)/3	$\Delta\varepsilon$'	$\Delta\varepsilon'/\varepsilon'_{\perp}$
Smectic A_d phase (24.0°C)	0	13.4	5.3	8.0	8.1	1.5
	6	13.5	5.4	8.1	8.1	1.5
	15	14.3	6.2	8.9	8.1	1.3
Nematic phase (34.0°C)	0	13.7	5.8	8.4	7.9	1.4
	6	14.4	5.8	8.7	8.6	1.5
	15	12.5	7.3	9.0	5.2	0.7

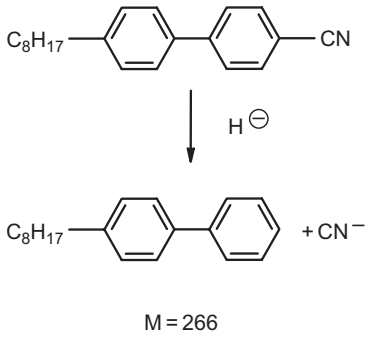

Figure 7. Formation of a low molecular product as a main destruction product due to electron beam irradiation.

revealed that in the smectic A_d phase, the longitudinal and transverse components of the relative dielectric permittivity and hence dielectric anisotropy ($\Delta\varepsilon'=\varepsilon'_{\parallel}-\varepsilon'_{\perp}$) are almost invariant even after irradiation up to 6 kGy dose. However, for the 15 kGy dose of irradiation both (the transverse as well as longitudinal) components increase compared with the pure sample. However, due to increase in both components of the relative dielectric permittivity, dielectric anisotropy remains invariant in the smectic A_d phase, even up to a 15 KGy dose of irradiation. In the nematic phase, dielectric anisotropy increases up to a 6 kGy dose of irradiation but decreases for a 15 kGy dose of irradiation (see Table 2).

Before explaining the above changes, it is important to mention here that the parameters $\Delta\varepsilon$' and $\varepsilon'_{\perp}$ play a vital role in the operation of TN-LCDs. The minimum voltage required for switching from the bright state (planar alignment) to the dark state (homeotropic alignment), i.e. threshold voltage (V_{th}), is inversely proportional to $\Delta\varepsilon$'. Therefore, for a low value of V_{th}, a

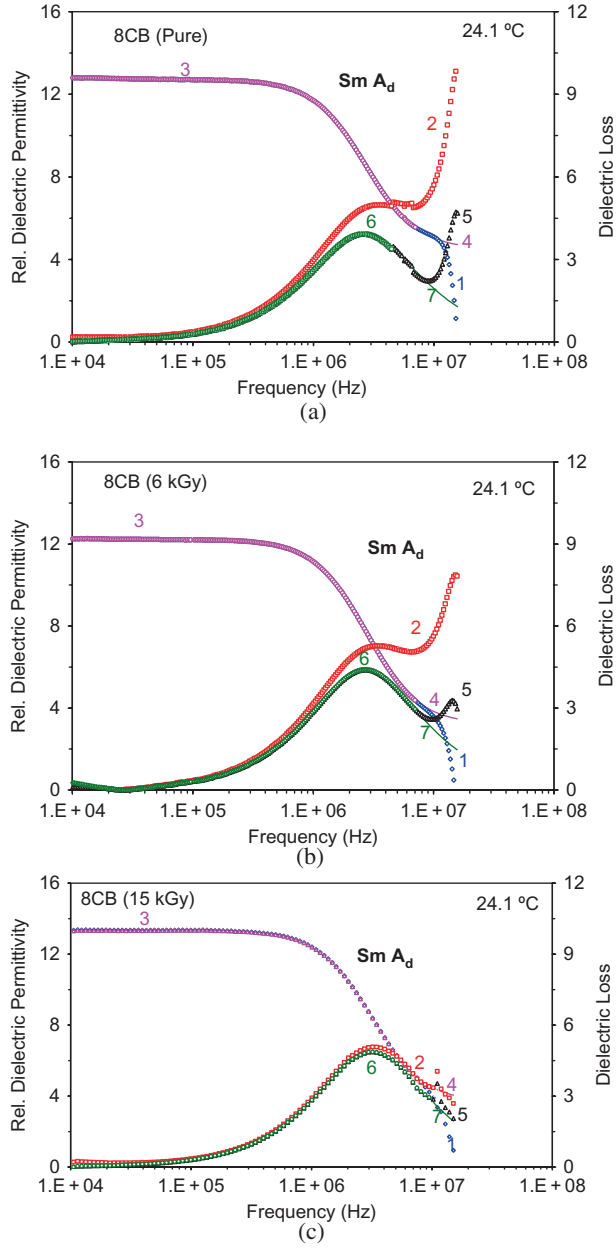

Figure 8. Frequency dependence of the longitudinal component of the relative dielectric permittivity ($\varepsilon'_{\parallel}$) and the dielectric loss ($\varepsilon''_{\parallel}$) in the smectic A_d phase (24.1°C). Curves 1 and 2 show the measured value of $\varepsilon'_{\parallel}$ and $\varepsilon''_{\parallel}$. Curve 3 shows the corrected measured data for $\varepsilon'_{\parallel}$ and curve 4 the generated data of $\varepsilon'_{\parallel}$. Curve 5 represents the corrected data of $\varepsilon''_{\parallel}$, obtained by subtracting the high frequency correction and low frequency correction from the measured data. Curve 6 shows the corrected measured data and curve 7 (thin line) shows the extension of the fitting curve to the experimental data of $\varepsilon''_{\parallel}$ to indicate the expected nature of the curve where correction is not effective. Curves 1, 3 and 4 are on the left vertical axis and 2 and 5–7 are on the right vertical axis. (a) 8CB pure sample; (b) 8CB (6 kGy) and (c) 8CB (15 kGy) electron beam-irradiated samples.

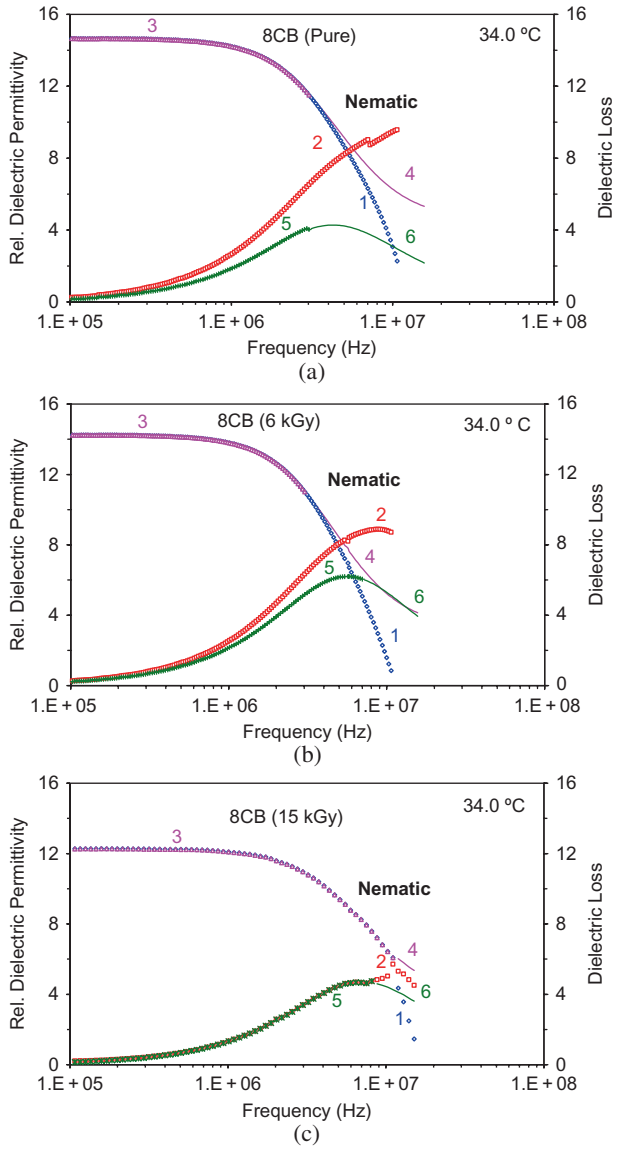

Figure 9. Frequency dependence of the longitudinal component of the relative dielectric permittivity ($\varepsilon'_{\parallel}$) and the dielectric loss ($\varepsilon''_{\parallel}$) in the nematic phase (34.0°C). Curves 1 and 2 show the measured value of $\varepsilon'_{\parallel}$ and $\varepsilon''_{\parallel}$. Curve 3 shows the corrected measured data for $\varepsilon'_{\parallel}$ and curve 4 the generated data of $\varepsilon'_{\parallel}$. Curve 5 represents the corrected measured data of $\varepsilon''_{\parallel}$ and curve 6 (thin line) shows the extension of the fitting curve to the experimental data of $\varepsilon''_{\parallel}$ to indicate the expected nature of the curve where correction is not effective. Curves 1, 3 and 4 are on the left vertical axis and 2, 5 and 6 are on the right vertical axis. (a) 8CB pure sample; (b) 8CB (6 kGy) and (c) 8CB (15 kGy) electron beam-irradiated samples. Experimental data (curves 1 and 2) are shown only up to 10 MHz as above that frequency, there is huge drop in the data, even into the negative, because of experimental limitations.

high positive value of $\Delta\varepsilon$' is required. At the same time the ratio of the parameters $\Delta\varepsilon'/\varepsilon'_{\perp}$ is responsible for the steepness of the transmission voltage curve (TVC). For low optical anisotropic materials, a low value of the ratio $\Delta\varepsilon'/\varepsilon'_{\perp}$ is necessary. Since, in the present case, the anisotropy increases (up to a 6 kGy dose of irradiation), hence it should decrease the threshold voltage. $\Delta\varepsilon'/\varepsilon'_{\perp}$ is almost invariant up to 6 kGy but decreases for a higher dose (15 kGy) of irradiation (see Table 2) and it may be helpful in improving the steepness of the TVC. Thus the parameters of the TVC can be optimised by choosing an appropriate dose of irradiation as obtained elsewhere (*8*).

The change in the dielectric parameters can be explained in terms of the formation of low molecular weight hydrocarbons due to the irradiation. The formation of such a hydrocarbon is shown in Figure 7. From the IR, MS and dielectric results we concluded that the CN group is detached from some 8CB molecules due to irradiation. It leaves behind impurities in the form of hydrocarbons of smaller molecular weight (see Figure 7). The presence of such hydrocarbons decreases the clearing point of the irradiated samples as compared with that of the pure sample. It also influences the dimerisation process of 8CB molecules. It is well known that *n*CB compounds exist partially in anti-parallel dimeric form $(8CB)_2 \rightarrow 2(8CB)$ (*19*). The presence of non-polar compounds influences the monomer-dimer equilibrium by increasing the monomer concentration. This occurs in the present case as well. Due to an increase in the 8CB monomers, $\varepsilon'_{\parallel}$ directly increases. The axis of the dipole moment of the CN coincides with the long axis of the 8CB molecule, but the net dipole moment of the whole molecule does not coincide with the long axis of the molecule. Therefore, destruction of the dimeric structure will affect both components (longitudinal as well as transverse) of the relative dielectric permittivity. This fact is visible in our dielectric data. At low dose, we see a small change (around 5%) in the components of the relative dielectric permittivity. However, at the higher dose (15 kGy), both components of the relative dielectric permittivity are substantially affected by the formation of above-mentioned hydrocarbon. It is also important to mention that the dipole moment of the detached CN group may not necessarily be along the long axis of the molecules. From Figures 5 and 6 we observe that the clearing point is substantially decreased and a broad biphasic region is observed. A low value of the longitudinal component of the permittivity of the 15 kGy irradiated sample in the nematic phase seems due to a high percentage of impurities created by the irradiation and also due to the biphasic region.

The transverse component of the relative dielectric permittivity of the material is constant in the frequency range of 100 Hz to 10 MHz for the planar-aligned (measuring field is normal to the director)

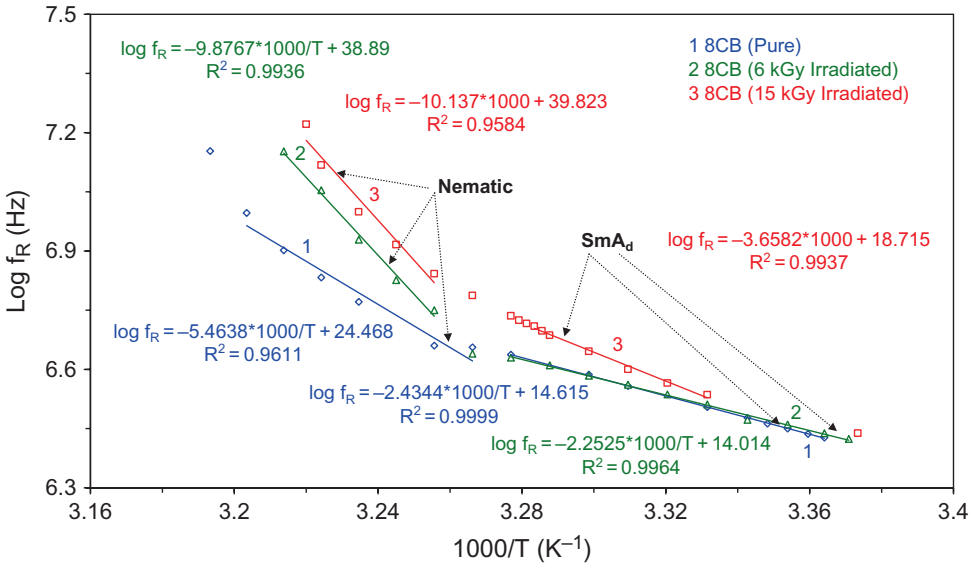

Figure 10. Variation of logarithmic of relaxation frequency ($\log f_R$) with the reciprocal of the absolute temperature (K^{-1}) in the smectic A_d and nematic phases. The rhombus is used for the pure sample, the triangle for 6 kGy and the square for 15 kGy dose electron beam-irradiated samples.

sample. This indicates that the relaxation frequency corresponding to the molecular rotation about its long axis cannot be detected in the experimental window of the frequency. However, we obtained a relaxation mode due to molecular rotation about its short axis. The variation of the relative dielectric permittivity and dielectric loss for the homeotropic-aligned molecules (measuring field along the director) are shown in Figures 8 and 9 for the smectic A_d and nematic phases, respectively.

The relaxation frequency of the pure 8CB is 2.672 MHz (±3 kHz) in the smectic A_d phase (at 24.1°C) and 4.571 MHz (±5 kHz) in nematic phase (at 34.0°C). The values of the relaxation frequencies in the smectic A_d and nematic phases are consistent with the data in the literature (*13*). The value of the relaxation frequency for the 6 kGy dose irradiated sample was found to be 2.701 MHz (±1 kHz) in the smectic A_d phase (at 24.1°C) and 5.624 MHz (±12 kHz) in nematic phase (at 34.0°C). For the 15 kGy dose irradiated sample, it was 3.148 MHz (±17 kHz) in the smectic A_d phase (at 24.1°C) and 6.954 MHz (±48 kHz) in nematic phase (at 34.0°C). From the comparison of relaxation frequencies of the pure and irradiated samples, we found the relaxation frequencies corresponding to molecular rotation about their short axes were increasing due to the irradiation. This can be understood in terms of the damage produced due to the irradiation as discussed in the previous paragraphs. When the CN group is detached from 8CB, the rest of the structure is no longer mesogenic and it may even decrease the order parameter of the system. Decrease in the order parameter may be responsible for the increase in the relaxation frequency. Conversion of dimers into monomers also decreases the inertia of the system and may increase relaxation frequency. The detached CN as well as the remaining hydrocarbon group act as impurities in the system and are responsible for the decrease in the clearing temperature due to the irradiation.

Relaxation frequencies (f_R) of the pure as well as those of the irradiated samples follow the Arrhenius behaviour given as

$$\log f_R = \log f_0 - W_A/RT \qquad (2)$$

where W_A is the activation energy, R is the universal gas constant, and T is the absolute temperature. Figure 10 shows the variation of the log of the frequency with the reciprocal of the absolute temperature. It is clear from Figure 10 that the log of the frequency with the reciprocal of the absolute temperature follows a linear behaviour with different slopes ($-W_A/R$) in different phases. Using least squares fit, slopes of the straight lines and consequently activation energies (W_A) were determined. For the pure 8CB, the results were 20.2 (±1.4) kJ mol^{-1} in the smectic A_d phase and 45.4 (±5.7) kJ mol^{-1} in the nematic phase. These values are in good agreement with the data in the literature (*13–16*). The activation energy of the 6 kGy dose irradiated sample was found to be 18.7±0.7 kJ mol^{-1} in the smectic A_d phase and 82.1 (±4.7) kJ

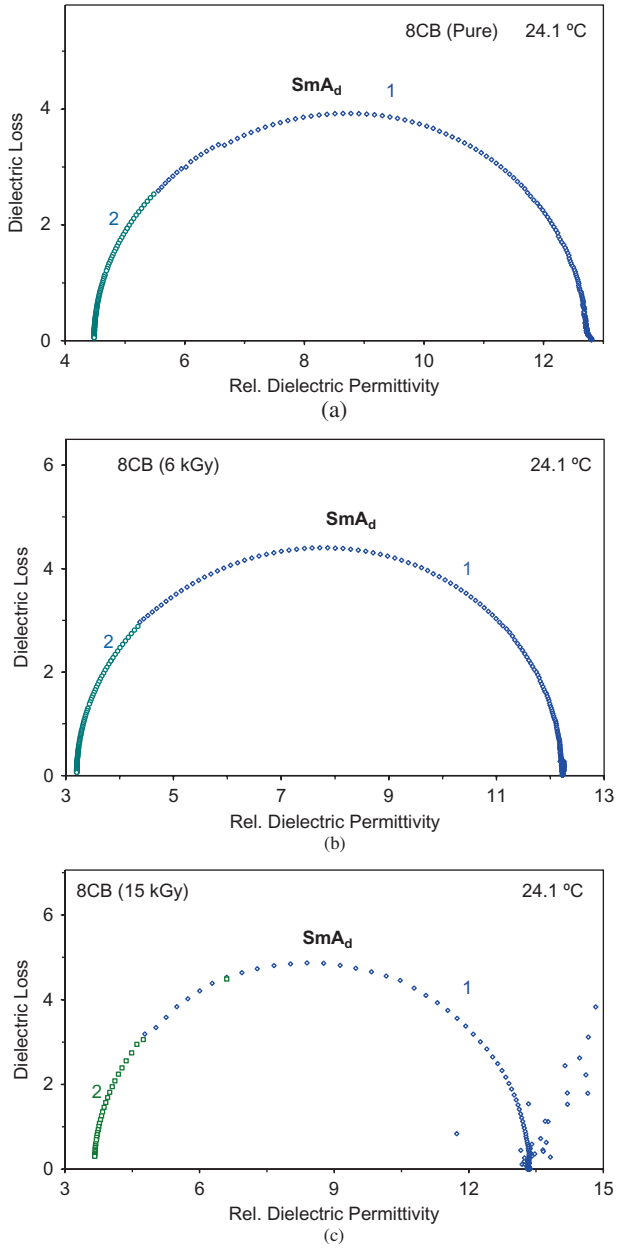

Figure 11. Cole–Cole plots showing the variation of dielectric loss with relative dielectric permittivity for the pure and irradiated samples in the smectic A_d phase (24.1°C). (a) 8CB pure sample; (b) 8CB (6 kGy) and (c) 8CB (15 kGy) electron beam-irradiated samples. Curves 1 and 2 represent the experimental and generated data, respectively.

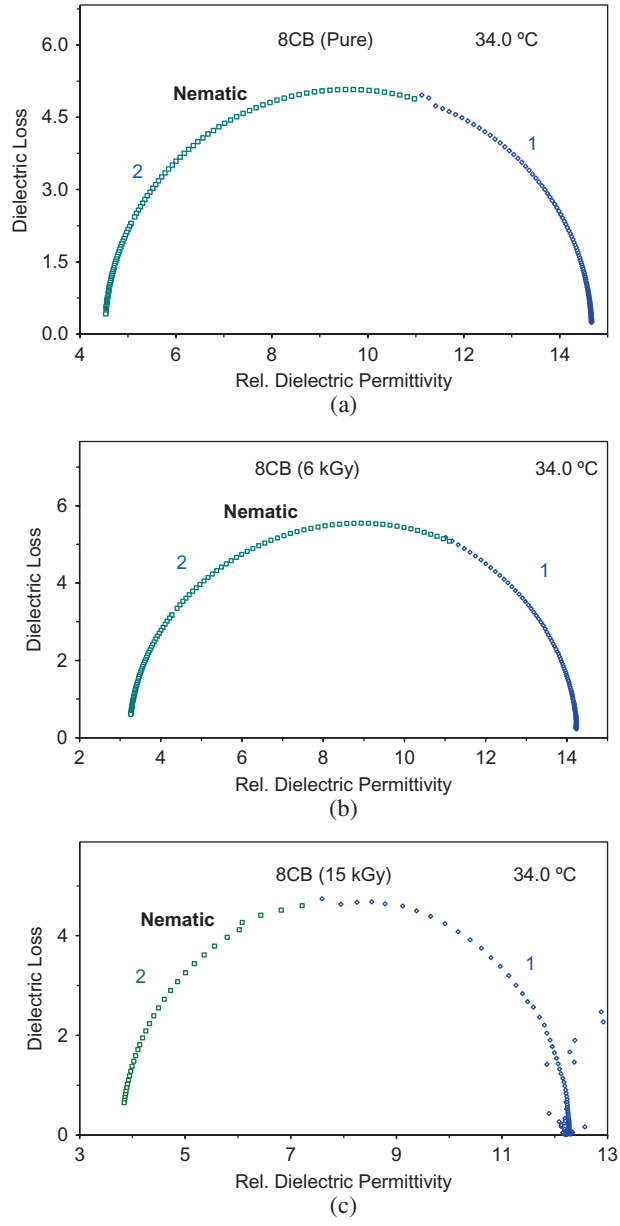

Figure 12. Cole–Cole plots showing the variation of dielectric loss with relative dielectric permittivity for the pure and irradiated samples in the nematic phase (34.0°C). (a) 8CB pure sample; (b) 8CB (6 kGy) and (c) 8CB (15 kGy) electron beam-irradiated samples. Curves 1 and 2 represent the experimental and generated data, respectively.

mol^{-1} in the nematic phase. For the 15 kGy irradiated sample, it was 30.4 (±2.0) kJ mol^{-1} in smectic A_d phase and 84.3 (±12.9) kJ mol^{-1} in the nematic phase. On comparison of the activation energies of the pure and irradiated samples, it was noticed that the activation energy tends to increase due to the irradiation except in the case of the smectic A_d phase of the 6 kGy irradiated sample where change was marginal.

The Cole–Cole plots showing the variation of the dielectric loss with relative dielectric permittivity in the smectic A_d (at 24.1°C) and nematic (at 34.0°C) phases are shown in Figures 11 and 12 for the pure and irradiated samples, respectively. From the Cole–Cole plots, which are complete semi-circles, the observed relaxation process is a typical Debye type and supports the relaxation process due to the rotation of individual molecules. The value of the α (around 0)

obtained from the fitting of Equation (1) with the dielectric data for pure and irradiated samples also supports the same result.

4. Conclusions

From the above experimental results and discussion, we were able to conclude the following.

Electron beam irradiation on 8CB molecules knocks out the CN group from some of the 8CB molecules and thereby produces a low molecular weight non-mesogenic system and CN group as impurities. Due to the formation of these impurities, the dielectric anisotropy of the irradiated sample increases for small doses, however, it decreases for higher doses of irradiation.

The relaxation frequencies of an observed relaxation mode corresponding to the flip-flop motion of the molecules about their short axis increases due to the irradiation.

It has been found that various parameters of the TVC can be optimised by choosing an appropriate dose of irradiation.

The observed results were supported by UV-visible, IR, GC and GCMS experiments. However, dielectric spectroscopy remains an important primary tool for the study of the consequences of irradiation effects.

Acknowledgements

The work was financially supported under a DAE-BRNS research project. RV thanks DAE-BRNS for a fellowship under a research project. VKW also acknowledges the DAE-BRNS for the award of a Raja Ramanna Fellowship. R Dh especially thanks the University Grants Commission, New Delhi, for granting leave exclusively for research work under the National Research Award scheme.

References

(1) Mauguin, C. *Bull. Soc. Franc. Min*. **1911**, *34*, 71–117.
(2) Alfassi, Z.B.; Kushelevsky, A.P.; Feldman, L. *Mol. Cryst. Liq. Cryst*. **1977**, *39*, 33–37.
(3) Klosowicz, S.J.; Alfassi, Z.B. *Mol. Cryst. Liq. Cryst.* **1994**, *239*, 181–193.
(4) Kurik, M.V.; Lavrentovich, O.D.; Linev, B.A.; Shulga, C.Z. *Sov. J. Chem. Phys.* **1987**, *61*, 1634–1636.
(5) Srivastava, S.L.; Dhar, R.; Kurik, M.V. *Mol. Mater*. **1993**, *2*, 261–273.
(6) Srivastava, S.L.; Dhar, R. *Radiat. Phys. Chem*. **1996**, *47*, 287–293.
(7) Srivastava, S.L.; Dhar, R.; Kurik, M.V. *Mol. Mater*. **2000**, *12*, 295–304.
(8) Dhar, R.; Verma, R.; Rath, M.C.; Sarkar, S.K.; Wadhawan, V.K.; Dabrowski, R.; Tykarska M. *Appl. Phys. Lett*. **2008**, *92*, 014108-1-3.
(9) Rath, M.C.; Sarkar, S.K.; Wadhawan, V.K.; Verma, R., Das, I.M.L.; Dabrowski, R.; Tykarska, M.; Dhar, R. *Opto Electron. Rev*. **2008**, *16*, 399–403.
(10) Hudson, K.; Ellman, B.; Gettwert, V.; Getmanenko, Y.; Twing, R.J. *Appl. Phys. Lett.* **2005**, *87*, 152103.
(11) Dunmur, D.A.; Manterfield, M.R.; Miller, W.H.; Dunleavy, J.K. *Mol. Cryst. Liq. Cryst*. **1978**, *45*, 127–144.
(12) Jadzyn, J.; Kedziora, P. *Mol. Cryst. Liq. Cryst*. **1987**, *145*, 17–23.
(13) Buka, A.; Price, A.H. *Mol. Cryst. Liq. Cryst*. **1985**, *116*, 187–195.
(14) Markwick, P.; Urban, S.; Wurflinger, A. *Z. Natureforsch.* **1999**, *54a*, 275–280.
(15) Urban, S.; Wurflinger, A.; Gestblom, B.; Dabrowski, R., Przedmojski, J. *Liq. Cryst.* **2003**, *30*, 305–311.
(16) Druon, C.; Wacrenier, J.M. *Ann. Phys.* **1978**, *3*, 199–214.
(17) Jin, M.Y.; Kim, J.J. *J. Phys. Condens. Matter* **2001**, *13*, 4435–4446.
(18) Parnix, J.P.; Legrand, C.; Decoster, D. *Mol. Cryst. Liq. Cryst.* **1983**, *98*, 361–374.
(19) Chakraborty, S.; Mukhopadhyay, A. *Phase Transitions* **2006**, *79*, 201–212.
(20) Guha, S.N.; Moorthy, P.N.; Kishor, K.; Naik, D.B.; Rao, K.N. *Proc. Indian Acad. Sci. (Chem. Sci.)* **1987**, *99*, 261–271.
(21) Srivastava, S.L.; Dhar, R. *Indian J Pure Appl. Phys*. **1991**, *29*, 745–751.
(22) Dhar, R. *Indian J. Pure Appl. Phys.* **2004**, *42*, 56–61.
(23) Srivastava, S.L. *Proc. Natl. Acad. Sci. India* **1993**, *63*, 311–324.
(24) Gouda, F.; Skarp, K.; Lagerwall, S.T. *Ferroelectrics* **1991**, *113*, 165–206.
(25) Gupta, M.; Dhar, R.; Agrawal, V.K.; Dabrowski, R.; Tykarska, M. *Phys. Rev. E* **2005**, *72*, 021703-1-9.
(26) Srivastava, A.K.; Agrawal, V.K.; Dabrowski, R.; Oton, J.M.; Dhar, R. *J. Appl. Phys*. **2005**, *98*, 013543-1-8.
(27) Pandey, M.B.; Dhar, R.; Agrawal, V.K.; Khare, R.P.; Dabrowski, R. *Phase Transitions*, **2003**, *76*, 945–958.